SECTION 3
CODE-PRESCRIBED ESTIMATION OF FUNDAMENTAL PERIODS

In order to estimate the lateral forces acting on a structure it is necessary first to estimate its fundamental period. Several factors contribute to the uncertainty of the estimation of fundamental periods from design plans, such as: variations in the modulus of elasticity, section dimensions, stripping operations, creep, and shrinkage. Over the life of the structure, cracks in structural members and disengagement of the partitions reduce the stiffness of the structure and lead to greater uncertainty of the periods. It is therefore difficult during the design stage to predict the dynamic properties of a structure at an arbitrary point in its service life. Without accurate estimates of fundamental periods, results from wind-tunnel experiments lead to inaccuracies in wind-related design requirements. Furthermore, the design base-shear for earthquake resistant design is a function of the structure's period. The applicable national or local Codes must be consulted to determine the empirical lower bound fundamental periods in order to establish the minimum lateral load requirements. It is apparent at this time that such Codes have not settled on a uniform method to determine the periods. The West Coast experience has been influencing this empirical approach which more accurately describes the stiffer structures designed to withstand large seismic forces in California. An exception is the earlier 1982 UBC Code.

The Uniform Building Code of 1982 specified that the period of a multi-story framed building can be estimated by dividing the total number of stories by ten [Blume, 1979]. This method results in longer periods than those measured in this study.

1982 UBC $\quad T = N/10 \quad (3.1)$

N = number of stories of the building

The 1988 version of the Uniform Building Code allows for one of two methods to be used in computing the natural period. The first method (Method A) takes the material of the building into account.

1988 UBC $T = C_t (h_n)^{3/4}$ (3.2)

$C_t = 0.020$ for dual moment resisting frames and eccentric braced frames;

$C_t = 0.1 / \sqrt{A_c}$ for structures with concrete or masonry shear walls;

$A_c = \sum A_e[0.2 + (D_e/h_n)^2]$ and depends upon the dimensions of the shear walls;

A_e is the minimum cross sectional shear area in any horizontal plane in the first story, in square feet, of a shear wall. D_e is the length in feet of shear wall in the first story in the direction parallel to the applied forces. A_c is the combined effective area, in square feet, of the shear walls of the first story of a structure. h_n is the effective height in feet above the base of the building [UBC 1988]. The effective height of the building, h_n, accounts for reduction in floor area at high floor levels, roof equipment, and elevator housings on the roof. The second method (Method B) specifies a Rayleigh-Ritz approach to determine the period.

East Coast experience has led to less stiff structures because of moderate lateral load requirements as well as the tendency of eastern construction to be taller and more slender. The proposed New York City seismic provisions modify the 1988 UBC Code by assigning $C_t = 0.035$ for frame concrete structures and by adjusting C_t for dual systems as follows:

$C_t = 0.020$ when $h_n \leq 160$ ft.

$C_t = 0.030$ when $h_n \geq 400$ ft.

Linear interpolation is permitted for intermediate heights.

This method results in shorter periods than those measured in this study. Table 3-I summarizes these results.

TABLE 3-I Comparison of Code-based Estimation of Fundamental Periods to the Measured Values in Ambient Conditions.

BLDG.	Height h_n	1982 UBC	1988 UBC (A)	Proposed NYC	Measured Ambient N-S	Measured Ambient E-W
A	486'	5.3 s	2.07 s	3.11 s	4.47 s	4.53 s
B	423'	4.1 s	1.87 s	2.80 s	3.98 s	2.79 s
C	249'	2.8 s	1.25 s	1.41 s	1.94 s	1.69 s
D	460'	4.9 s	1.99 s	2.98 s	3.76 s	3.88 s

In comparing periods from code equations with measured ambient periods, it should be noted that the equations in the design code are meant to describe the structure in its ultimate state, for example, story drift of H/200, whereas the measured ambient periods correspond to story drifts of much less than H/1000. Stiffness degradation at larger story drifts will result in longer periods than those measured when the building is in ambient conditions.

Note that the code equations are really not meant to provide accurate estimates of the fundamental period, but for finding the proper design force level, as prescribed by a design spectrum. To be conservative, the periods from code formulas should therefore be less than the measured periods under ambient conditions, which applied in the 1988 UBC Code and the proposed NYC Seismic Code. (See Table 3-I.)

SECTION 4
INSTRUMENTATION AND MEASUREMENT PROCEDURES

In all four buildings, Terra Technology SSA-302 triaxial force-balance accelerometers were the sensors used to measure horizontal and vertical accelerations at various floor levels. Kinemetrics 5-second seismometers were used to measure the velocity motion of the foundation. The Terra Tech accelerometers exhibit excellent linearity by virtue of the feed-back control of the seismic mass. In addition, the fluid damped design makes them very rugged. Triaxial accelerometers were placed at different floor levels in the buildings. Two triaxial accelerometers on the same floor near the top of the building allowed the identification of torsional modes. In buildings A and B, the deployed accelerometers measured to ±0.2g full scale. In buildings C and D, the accelerometers measured to ±2.0g full scale. PRS-4 synchronous, digital, 12-bit, auto-scaling, battery powered recorders sampled, digitized, and recorded the data. Each recorder has 1 Mega-byte of RAM for data storage. There was one PRS-4 recorder per triaxial accelerometer. The PRS-4's are especially well suited for temporary instrumentation of large scale structures because they have synchronized (±1 milli-second) internal clocks, therefore they can operate independently from one another, do not require any interconnecting cables, and are ruggedized. The PRS-4 units were pre-programmed to sample simultaneously at a pre-specified time of day, sample rate, and duration. The wind was very light during the measurements of buildings A and B but was 35 knots during the measurements of buildings C and D. This is evidenced by much heavier participation of the lower frequencies for buildings C and D. The following table summarizes the instrumentation location and the data acquisition on the four structures. In Table 4-I, B stands for basement, E and W for east and west positions of the floor plan. Sensor locations not in either the east or west positions were placed near the center of the floor plan.

TABLE 4-I Measurement Locations and Data Acquisition

BLDG.	SENSOR LOCATIONS - FLOOR NUMBER							SAMPLE RATE	TIME
A	B	10	20	30	40	52E	52W	50 / sec	20 min.
B	B	10	20	30	36E	36W	40	25 / sec	40 min.
C	B	6	28	29E	29W			25 / sec	30 min.
D	B	10	51	51E	51W			25 / sec	30 min.

Measurements from Building A were taken on February 4, 1991; those from Building B were taken on February 7, 1991. Buildings C and D were measured on February 22, 1991. Buildings A and B were measured a second time on August 15, 1991. Appendix B contains the results from the first set of measurements. For completeness, the results from the second set of measurements are included in Appendix C.

After each test, the data was transferred via a Compaq portable PC to a network of Sun Spark stations for analysis. After formatting the data into the proper ASCII format, auto-power and phase spectra were estimated. Peak picking software facilitated the spectral analysis.

SECTION 5
DATA ANALYSIS AND SPECTRAL PARAMETER ESTIMATION

Ideally, estimation of the parameters of a system is accomplished by fitting a model of the system to simultaneously sampled input and output data records. While the costs associated with artificial, measurable excitation of civil engineering structures are high, parameters estimated from forced-vibration tests are accurate and indicative of the nature of the structure itself [Ho 1989]. The force-levels required for uniform excitation of high-rise structures requires expensive and elaborate test arrangements, including reaction-mass servo-hydraulic actuators in many cases. Furthermore, forcing the structural response to levels significantly greater than ambient levels may risk non-linear behavior and subsequent damage to the structure, if measurement feedback is not used to limit the actuator excitation. Because of these experimental difficulties, and in light of the relative ease of collecting ambient vibration measurements as described in Section 4, the four high-rise structures were measured in ambient conditions.

If certain assumptions regarding the characteristics of the excitation to the structure, the structural behavior, and the response measurements hold, then the analysis of ambient vibration measurements will yield more meaningful results [Luz, 1992]. These assumptions are:

1. The excitation is sufficiently broad band and stochastic to uniformly excite at least the lowest 20 to 30 modes of the three-dimensional structure. In each of these structures the lower resonant frequencies range from 0.2 Hertz to 5 Hertz. Spatially uncorrelated excitations also helps reduce the chances of disproportionate energy concentration in certain modes.
2. The measured acceleration responses are at least weakly stationary. This permits meaningful time averages of the auto-power and cross-power spectra. The response

will be stationary if the excitation (wind pressure) is stationary, and the structure behaves linearly.

3. The resonant modes are lightly damped and the resonant frequencies are distinct and well separated. In this condition, spectral peak amplitudes have negligible contribution from out-of-band resonances. The figures in Appendices B and C verify that these assumptions hold.
4. Samples of the vibration measurements are simultaneous in time at all measurement locations. This condition is essential for proper cross-power spectral estimation. The test hardware guarantees nearly simultaneous sampling, as is indicated in Section 4.

If the above assumptions are warranted, frequencies with maximum spectral power (peak frequencies) can be interpreted as structural natural frequencies. In ambient conditions, tall buildings in urban areas are excited by wind turbulence and mechanical equipment. Wind pressures are spatially and temporally less correlated in turbulent flow than in laminar flow, but the spectra of turbulent velocity fluctuations decreases logarithmically with frequency [Simiu and Scanlan 1986]. Wind pressures are not uniformly distributed along the height of these high-rise structures. And because many of these buildings rise above the surrounding structures, the spectrum of wind velocites near the tops of the buildings can be qualitatively different from those in the lower stories. Since the auto-power spectra can not be normalized by the (unmeasured) wind forces, the spatial distribution of structural vibrations corresponding to a particular modal frequency are termed "operational deflection shapes." An operational deflection shape (ODS) is defined as the spatial distribution of peak spectral amplitudes at a resonant frequency.

Parameter estimation methods that implement an input-output ARMA model of the system were tested for ambient vibration applications [Ghanem, 1991]. However, the parameters resulting from such methods often depend upon assumptions regarding initial conditions, excitation, and

measurement noise. In addition, these methods are more computationally intensive than methods based on the Fast Fourier Transform (FFT). Frequency domain analysis is especially useful for ambient vibration data, since the long durations of data allow for a considerable amount of averaging while maintaining a very high resolution of frequencies. Small frequency increments, Δf, are necessary to characterize low frequency peaks. Computer programs tailored for spectral estimation from multi-measurement ambient data were written to first estimate power and phase spectra, then use these spectra to pick the peak frequencies, amplitudes, and to estimate damping, RMS acceleration, RMS velocity, and RMS displacement. To verify the operation of the programs described above, an almost identical method was implemented independently at Columbia University's Lamont-Doherty Geological Observatory. Consistent results confirmed the accuracy of the programs.

5.1 Spectrum Estimation

Acceleration data are digitized and sampled with a sample interval of Δt seconds. $a(t) = a(i\Delta t)$, $i=1...P$, where P is the total number of points in the digitized data record. The data record is divided into K overlapping sample functions, a_k, $k=1...K$, of N (a power of 2) points each. The sample functions overlap each other by 50% of their length.

$$a_k(i\Delta t) = a((j+i)\Delta t), \quad j = \frac{N(k-1)}{2}, \quad k=1\cdots K, \quad i=1\cdots N \tag{5.1}$$

Each sample function is multiplied by the Hanning window, w .

$$\tilde{a}_k(i\Delta t) = a_k(i\Delta t)\, w_i \tag{5.2}$$

$$w_i = \frac{1}{2} - \frac{1}{2}\cos\left(\frac{2\pi(i-1)}{N-1}\right) \tag{5.3}$$

The complex valued discrete Fourier transform (DFT) of each segment is computed using the Cooley-Tukey (decimation in time) algorithm with the Danielson-Lanczos lemma to calculate

the transforms [Oppenheim 1979, Press 1988]. This radix-2 method of computing the discrete Fourier transform is one of a variety of Fast Fourier Transform (FFT) methods. The Fourier transform is defined for both positive and negative frequencies. K FFT's are computed from each of two time records: a response acceleration record, $y(i\Delta t)$, at an elevated floor; and a reference acceleration record, $x(i\Delta t)$ near the base of the building. For proper phase spectrum estimation, it is essential that the samples for the x and y time records be simultaneous. Each record is segmented and windowed as the FFT's, $\widetilde{X}_k$ and $\widetilde{Y}_k$, are computed. Windowing the data reduces the leakage error in the FFT.

$$\widetilde{X}_k(j\Delta f) = \sum_{i=1}^{N} \widetilde{x}_k(i\Delta t) e^{-i\,2\pi ij/N} \tag{5.4}$$

$$\widetilde{Y}_k(j\Delta f) = \sum_{i=1}^{N} \widetilde{y}_k(i\Delta t) e^{-i\,2\pi ij/N} \tag{5.5}$$

Where the italic "*i* " in the exponent is the imaginary number and should not be confused with the non-italic index, "i." The discrete frequency interval is $\Delta f = 1/(N\Delta t)$, and j=1...N/2. The discrete, one-sided, auto power spectrum, $G_{yy}(j\Delta f)$, and cross power spectrum, $G_{xy}(j\Delta f)$, are computed by averaging the auto-power and cross power spectra of the K overlapping sample functions.

$$G_{yy}(j\Delta f) = \frac{1}{NK\sum_{i=1}^{N} w_i^2} \sum_{k=1}^{K} \left[\left|\widetilde{Y}_k(j\Delta f)\right|^2 + \left|\widetilde{Y}_k(-j\Delta f)\right|^2 \right] \tag{5.6}$$

$$G_{xy}(j\Delta f) = \frac{1}{NK\sum_{i=1}^{N} w_i^2} \sum_{k=1}^{K} \left[\widetilde{X}_k(j\Delta f)\widetilde{Y}_k^*(j\Delta f) + \widetilde{X}_k^*(-j\Delta f)\widetilde{Y}_k(-j\Delta f) \right] \tag{5.7}$$

The asterisk (*) indicates the complex conjugate of the variable. The factor in the denominator of equations (5.6) and (5.7) results in a normalization such that

$$\sum_{j=1}^{N/2} G_{yy}(j\Delta f) = \frac{1}{P}\sum_{i=1}^{P} [y(i\Delta t)]^2 \qquad (5.8)$$

The phase spectrum is calculated using the cross power spectrum with respect to the lowest measured floor (usually the tenth in these buildings). The discrete phase spectrum, $\theta(j\Delta f)$ is defined by

$$\theta(j\Delta f) = \arctan\left(\frac{\mathrm{Re}(G_{xy}(j\Delta f))}{\mathrm{Im}(G_{xy}(j\Delta f))}\right) \qquad (5.9)$$

The phase spectrum evaluated at peak frequencies of the auto power spectrum is almost always within 5° of either 0° or 180°. The power and phase spectra are given in Appendix B. The results of an analysis of a second set of measurements for Buildings A and B are included in Appendix C. Program AMB, listed in Appendix D, computes the auto-power spectrum and the phase spectrum given a pair of vibration records.

5.2 Parameter Estimation

Structural resonant frequencies are estimated in each auto spectrum by curve-fitting a quadratic to the three largest values in the regions of peak spectral power, and calculating the coordinates of the peak of the quadratic. The curve-fit is exact since three points uniquely determine a quadratic; no least squares or maximum likelihood methods are needed for this estimation. Since the power and phase spectra are not transfer or transmittance functions, traditional modal analysis curve-fitting methods [Ho 1989, Richardson 1982, Richardson 1985, Vold 1990] cannot be employed, nor can many other methods which rely on an input-output model of the structure [DiPasquale 1987, Ewins 1984, Ghanem 1991, Ho 1989]. Nevertheless, since points in the power spectrum are usually asymmetrically spaced around the peak frequency, the frequency of the true largest power spectrum value usually does not coincide with the sampled peak frequency; the true peak frequency is usually within one frequency interval of the largest

data value (see Figure 5-1.) By fitting a quadratic to the three largest points in the spectrum, the peak coordinates may be estimated easily.

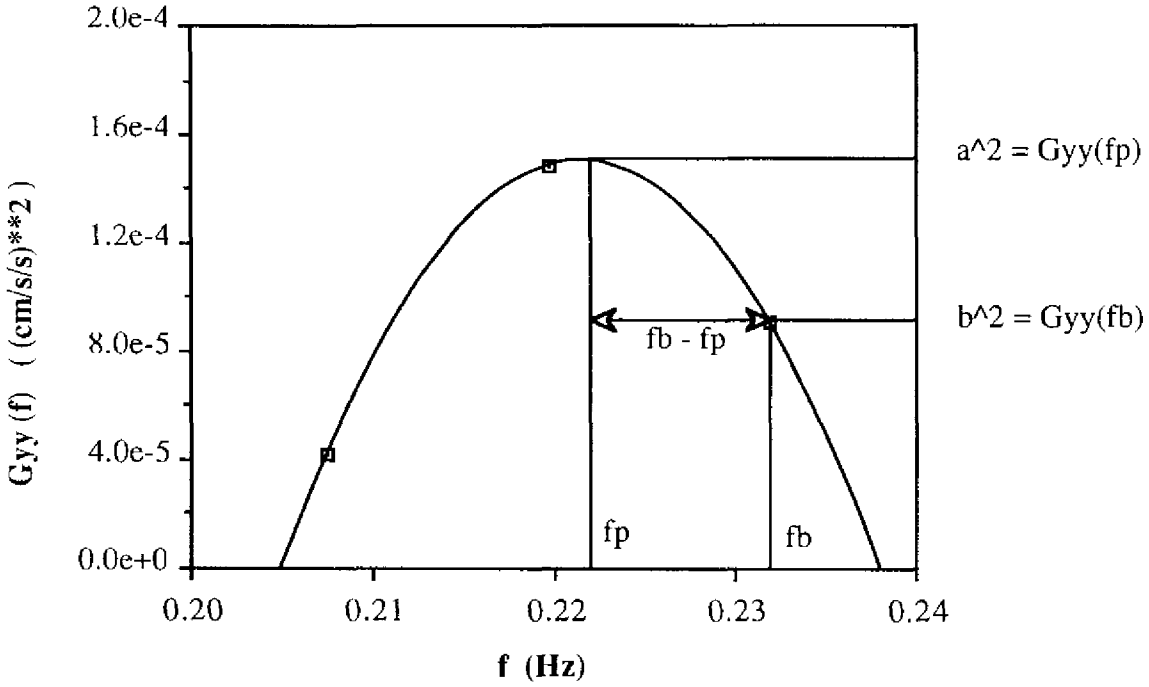

Figure 5-1 Quadratic Curve-fit to the Auto-power Spectral Peak

$G_{yy}(f) = c_0 + c_1 f + c_2 f^2$

Peak Frequency: $f_p = c_1 / (2c_2)$, Peak Amplitude: $G_{yy}(f_p) = c_0 + c_1^2 / (4c_2)$.

The variables a^2 and b^2 are used in Appendix A.

Given the coordinates of the largest sampled peak, $(f_2, G_{yy}(f_2))$, and the two adjacent coordinates, $(f_1, G_{yy}(f_1))$ and $(f_3, G_{yy}(f_3))$, a quadratic, $G_{yy}(f) = c_0 + c_1 f + c_2 f^2$, passing through all three points is computed by solving

$$\begin{Bmatrix} G_{yy}(f_1) \\ G_{yy}(f_2) \\ G_{yy}(f_3) \end{Bmatrix} = \begin{bmatrix} 1 & f_1 & f_1^2 \\ 1 & f_2 & f_2^2 \\ 1 & f_3 & f_3^2 \end{bmatrix} \begin{Bmatrix} c_0 \\ c_1 \\ c_2 \end{Bmatrix} \tag{5.10}$$

for c_0, c_1, and c_2 using Gauss-Jordan inversion with partial pivoting. The estimated peak frequency is $f_p = c_1 / (2c_2)$. The estimated peak amplitude is $G_{yy}(f_p) = c_0 - c_1^2 / (4c_2)$.

The structural damping ratio is calculated using the band-width of the auto power spectrum. The peak coordinate estimated from the curve-fit, $G_{yy}(f_p)$, and the auto power spectrum data at a point near the half-peak level, $G_{yy}(f_b)$, are used to compute the damping ratio (refer to Figure 5-1). Band-width formulae for computing damping ratios are derived from the analytic expression of the dynamic amplification factor of a SDOF structure under steady-state harmonic motion (for details see Appendix A). The amplification factor is defined in terms of displacements and assumes viscous damping [Beards 1983, Paz 1985]. Since our power spectra are computed from acceleration data, and the normalization is given by equation (5.8), dividing each point by $(2\pi f)^4$ results in displacement spectra. Assuming that the structure behaves linearly, has viscous damping, and has a stationary, steady-state, narrow-band response, that acceleration power spectra are normalized as in equation (5.8), and that the computed auto-power spectrum has no bias or leakage errors, then the following expression results in an approximate damping estimate.

$$\zeta = \frac{|f_b - f_p|}{f_p \sqrt{\left(\frac{f_b}{f_p}\right)^4 \frac{G_{yy}(f_p)}{G_{yy}(f_b)} - 1}} \qquad (5.11)$$

The curve-fit peak coordinate is $(f_p, G_{yy}(f_p))$; the coordinate at the band-width level is $(f_b, G_{yy}(f_b))$. The band-width frequency coordinate, f_b, is always taken to be greater than the peak frequency, f_p; and the band-width amplitude is no greater than 70% of the peak amplitude. This method of frequency estimation and damping calculation allows for the frequency data to be asymmetrically spaced around the peak and uses exact data values when appropriate. Equation (5.11) is a conservative approximation which ignores higher order terms (see Appendix A). Recently, FFT-based averaged spectrum estimation methods have been applied

to the problem of damping estimation of long span suspension bridges [Jones 1990, Littler 1991].

For finite lengths of data, there is a trade-off between the error in the spectral amplitudes and the spectral resolution of any FFT-based spectrum estimation routine [Gade 1988]. The variance of a spectrum with fine spectral resolution is larger than the variance of an averaged spectrum with coarse spectral resolution computed from a data set of a fixed length [Press 1988]. The normalized standard error of a spectral estimate is $K^{-1/2}$, where K is the number spectral averages [Bendat 1986]. However, spectral bias errors result from averaging spectra and have the effect of widening spectral peaks. An estimate of the bias error of a spectral estimate is $E_b = -\Delta f/(6\zeta f)^2$ where Δf is the frequency resolution of the spectrum, and f and ζ are the frequency and damping ratio associated with a peak in the spectrum [Bendat 1986]. The bias can be somewhat controlled by the shape of the window function. In choosing a window function, there is a trade off between the narrowness of the peak and side-lobe amplitudes; so windows that produce narrow peaks are not always advantageous. Other spectrum estimation methods, employing multiple orthogonal window functions, have been shown to reduce bias errors more effectively [Thompson 1982, Park 1987].

In an effort to find the combination of the window function and number of averages which gives a spectrum with an appropriate band-width, several approaches were employed. All approaches used the same simulated acceleration response record of a linear SDOF system of a known natural frequency and damping ratio. The linear acceleration method was used to simulate the acceleration response record [Paz 1985]. Spectra of the resulting simulated acceleration response record were computed using various window functions and numbers of averages. Method 1 simply compared the known damping ratio to the damping ratio computed using equation (5.11). Methods 2 and 3 compared the bandwidth factor, q, computed from a closed form solution to the band-width factors computed from spectral moments, equation

(5.13), and from envelope statistics, equation (5.14). Three expressions of the band-width factor, q, are [Vanmarcke 1972]

$$q^2 = 1 - \frac{1}{1-\zeta^2}\left[1 - \frac{1}{\pi}\tan^{-1}\left(\frac{2\zeta\sqrt{1-\zeta^2}}{1-2\zeta^2}\right)\right]^2 \tag{5.12}$$

$$q^2 = 1 - \frac{\lambda_1^2}{\lambda_0\lambda_2} \tag{5.13}$$

$$q = \frac{\sigma_{\dot{r}}}{\sigma_{\dot{x}}} \tag{5.14}$$

where ζ is the damping ratio, and λ_i is the i^{th} spectral moment of the auto-power spectrum.

$$\lambda_i = \sum_{j=1}^{N/2} (j\Delta f)^i G_{yy}(j\Delta f) \tag{5.15}$$

$\sigma_{\dot{r}}$ and $\sigma_{\dot{x}}$ are computed using envelope statistics. $\sigma_{\dot{r}}$ and $\sigma_{\dot{x}}$ are the standard deviations of the time rates of change of the random processes x and r respectively. The envelope of the random process is r, and x is computed as the modulous of the complex quantity $x + i\,\hat{x}$, where $\hat{x}$ is the Hilbert transform of x and can be computed in the frequency domain or in a finite impulse response filter form in the time domain [Bendat 1986, Boashash 1987, Deutsch 1969, Rao 1990]. The impulse response function of the Hilbert transform is

$$h(t) = \frac{1}{\pi t} \tag{5.16}$$

The Fourier transform of $\hat{x}(t)$ is $\hat{X}(f)$ and the Fourier transform of x(t) is X(f).

$$\hat{X}(f) = \begin{Bmatrix} i\,X(f) & \text{if } f > 0 \\ 0 & \text{if } f = 0 \\ -i\,X(f) & \text{if } f > 0 \end{Bmatrix} \tag{5.17}$$

After computing $\hat{X}(f)$ from equation (5.17), $\hat{x}(t)$ is computed using the inverse Fourier transform of $\hat{X}(f)$. The time derivatives of the processes are computed using the central difference rule.

$$\dot{x}_J = \frac{x_{J+1} - x_{J-1}}{2\Delta t} \qquad (5.18)$$

Figure 5-2 shows a portion of the simulated acceleration response record, its envelope function, and the power spectrum of the simulated acceleration record.

No combination of window function and frequency interval resulted in a very good match for all three methods of band-width comparison simultaneously. The final decision on what level of averaging and window function to use was based largely on the results from Method 1. Since the frequency values are of much greater interest in this study, a finer spectral resolution was favored. From these considerations, a frequency interval of approximately 0.0061 Hz and the Hanning window function were chosen to be suitable. This resulted in 13 spectral averages for Building A, 28 spectral averages for Building B, 20 averages for Building C, and 20 for Building D. A more rigorous analysis would take advantage of multi-taper methods [Park 1987, Thompson 1982] and would be an interesting topic for further study. These methods result in spectral estimates which have much smaller bias errors.

In summary, spectral band-widths can be determined to a large extent by computational errors in peak regions of the spectrum. If the auto-power spectrum is calculated with little regard to the sources of these errors, damping estimates from band-width measures may have little physical significance. In addition, damping estimates from band-width measures of ambient vibration data are contingent upon implicit assumptions, are subject to data processing effects, and therefore are used only as comparative measures within this analysis.

5.3 Root-Mean-Square Computations

Since the auto power spectra are normalized as in equation (5.8), the square root of the sum of the power spectrum points is the root-mean-square acceleration of the record, provided that the

time history was demeaned or high-pass filtered prior to power spectrum computation. More importantly, however, root-mean-square velocity or displacement can be obtained if each spectral data point is divided by $(2\pi f)^2$ or $(2\pi f)^4$, respectively. Root mean squared displacement computations in the frequency domain are contingent upon the following assumptions:

1. The original discrete acceleration record can be represented by a Fourier series expansion.
2. Each power spectrum coordinate equals the amplitude squared of the corresponding Fourier series term.
3. Term by term integration of the Fourier series representing the acceleration record results in a Fourier series representing the velocity record. And term by term integration of the Fourier series representing the velocity record represents the displacement record.

Root-mean-squared (RMS) displacement computations are most sensitive to low-frequency accelerations. Power spectra often contain low frequency biases due to low-frequency noise in the measured acceleration records. Since low-frequency biases in the power spectrum result in gross over-estimates of RMS velocity and especially RMS displacement, all power spectrum values below 1 rad/sec (0.159 Hz) are divided by 1 instead of $(2\pi f)^2$ or $(2\pi f)^4$, thereby attenuating the very low-frequency noise. (For small values of f, the function $1/(2\pi f)^4$ becomes very large.) 1 rad/sec (Period = 6.28 sec) is a reasonable lower bound for structural oscillations of the buildings in this study. The equations for frequency domain calculation of the root mean square equations are:

$$\text{RMS-acc} = \left[\sum_{j=1}^{N/2} G_{yy}(j\Delta f)\right]^{\frac{1}{2}} \tag{5.18}$$

$$\text{RMS-vel} = \left[\sum_{j=1}^{N/2} \frac{G_{yy}(j\Delta f)}{\omega^2} \right]^{\frac{1}{2}} \tag{5.19}$$

$$\text{RMS-dsp} = \left[\sum_{j=1}^{N/2} \frac{G_{yy}(j\Delta f)}{\omega^4} \right]^{\frac{1}{2}} \tag{5.20}$$

where

$$\omega = \left\{ \begin{array}{l} 2\pi j\Delta f \text{ if } j\Delta f \geq 0.159 \\ 2\pi\, 0.159 \text{ if } j\Delta f < 0.159 \end{array} \right\} \tag{5.21}$$

Alternately, integrating acceleration time histories numerically results in velocity and displacement time histories. Numerical integration can be unstable if the record to be integrated contains frequencies greater than $1/(4\Delta t)$ Hz [Hamming 1989]. To estimate RMS displacement from recorded acceleration time records, the authors found that the following procedure was sufficiently accurate:

1. Demean the acceleration time record by subtracting the average acceleration from all data points.
2. Low-pass filter the acceleration time record with a cut-off frequency at $1/(5\Delta t)$ Hz. A non-recursive Kaiser filter was implemented in these analyses [Hamming 1989].
3. Integrate the demeaned, filtered, acceleration data once using Tick's rule [Hamming 1989]. Tick's rule is accurate and stable up to $1/(4\Delta t)$ Hz.
4. Band-pass filter the integrated acceleration record between 0.15 Hz and $1/(5\Delta t)$ Hz.
5. Integrate again using Tick's rule and find the RMS value of the 'displacement' time record.

These methods were verified in the laboratory by measuring and recording simultaneous acceleration and displacement time histories of a SDOF system excited randomly by base accelerations. A linear voltage displacement transducer (LVDT) measured the mass's

deflections while a force balance accelerometer measured the mass's accelerations. RMS displacement was computed in three ways: directly from the recorded displacement time records, in the frequency domain using the acceleration power spectrum and equations (5.20) and (5.21), and in the time domain from the five-step process outlined above. The resulting RMS values were within 2% of each other. Comparable results between the time and frequency domain methods using the ambient vibration data collected from the measured structures in New York City provided further confirmation of the accuracy of the frequency domain approach. Table 5-I compares the measured RMS displacement and the computed RMS displacements for the SDOF structure tested in the laboratory. RMS displacement values computed from the 52nd floor of Building A are indicated in the second row of Table 5-I.

TABLE 5-I Validation of the Frequency Domain RMS Computation Method

	Measured Displacement	Frequency Domain	Time Domain
SDOF-RMS	0.591 in.	0.588 in.	0.578 in.
NYC - RMS		0.112 cm	0.130 cm

To facilitate the analysis of the power spectra and phase spectra computed by program AMB, program PEAK was written. This program passes through the spectral data several times to compute RMS quantities, pick peaks, sort the peaks by increasing frequency, fit a quadratic to the peaks, and estimate values for the peak frequencies, amplitudes, and damping ratios. To qualify as a peak, the power spectrum data must satisfy all of the following conditions:

1. The power spectrum frequency coordinate must lie within a user-specified frequency band.
2. The amplitude must be larger than any other point not already identified as a peak.

3. The derivative of the spectrum with respect to frequency must change signs at a peak.
4. The frequency at a peak must be outside of a user-specified frequency buffer around any previously identified adjacent peak. This helps in eliminating picking large side-lobes as legitimate peaks.

In estimating the damping ratio, the spectral coordinate used for the band-width estimation is no greater than 70% of the peak amplitude. The source code for program PEAK is included in Appendix E.

FIGURE 5-2

Simulated Acceleration Response, Computed Envelope, and Estimated Power Spectrum